

PRIGo: a new multi-axis goniometer for macromolecular crystallography

Sandro Waltersperger,^{a,†} Vincent Olieric,^{a,*} Claude Pradervand,^a Wayne Glettig,^b Marco Salathe,^a Martin R. Fuchs,^{a,§} Adrian Curtin,^a Xiaoqiang Wang,^a Simon Ebner,^a Ezequiel Panepucci,^a Tobias Weinert,^a Clemens Schulze-Briese^c and Meitian Wang^{a,*}

Received 14 November 2014

Accepted 15 March 2015

Edited by I. Schlichting, Max Planck Institute for Medical Research, Germany

† These authors contributed equally to this work.

§ Present address: NSLS-II, Brookhaven National Laboratory, Upton, NY 11973, USA.

Keywords: multi-axis goniometry; macromolecular crystallography; diffractometer; diffraction data; collection strategy; beamline endstation.

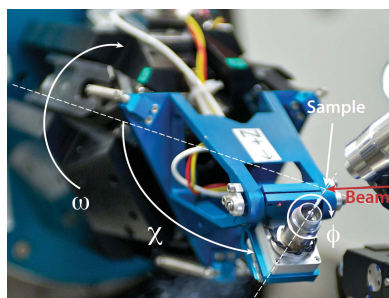
^aSwiss Light Source, Paul Scherrer Institute, Villigen PSI, Switzerland, ^bCentre Suisse d'Electronique et Microtechnique SA, Neuchâtel 2002, Switzerland, and ^cDectris Ltd, Baden 5400, Switzerland.

*Correspondence e-mail: vincent.olieric@psi.ch, meitian.wang@psi.ch

The Parallel Robotics Inspired Goniometer (PRIGo) is a novel compact and high-precision goniometer providing an alternative to (mini-)kappa, traditional three-circle goniometers and Eulerian cradles used for sample reorientation in macromolecular crystallography. Based on a combination of serial and parallel kinematics, PRIGo emulates an arc. It is mounted on an air-bearing stage for rotation around ω and consists of four linear positioners working synchronously to achieve x, y, z translations and χ rotation ($0\text{--}90^\circ$), followed by a φ stage ($0\text{--}360^\circ$) for rotation around the sample holder axis. Owing to the use of piezo linear positioners and active correction, PRIGo features spheres of confusion of $<1\ \mu\text{m}$, $<7\ \mu\text{m}$ and $<10\ \mu\text{m}$ for ω , χ and φ , respectively, and is therefore very well suited for micro-crystallography. PRIGo enables optimal strategies for both native and experimental phasing crystallographic data collection. Herein, PRIGo hardware and software, its calibration, as well as applications in macromolecular crystallography are described.

1. Introduction

The success of a macromolecular crystallography (MX) diffraction experiment depends on the accurate measurement of intensities and the completeness of the data. The main causes of failure are overlapping reflections (Dauter, 1999), radiation damage (Blake & Phillips, 1962; Ravelli & Garman, 2006; Garman & Weik, 2011) and noise originating from various sources (Holton & Frankel, 2010). Consideration and optimization of these parameters are crucial for obtaining the best outcome (Dauter, 2005, 2010). To this end, crystallographers have always employed data collection protocols involving crystal alignment using multi-axis goniometers. They are still routinely used on X-ray laboratory sources to obtain complete data sets at high resolution from small molecule crystals (Helliwell, 1992). At synchrotron MX beamlines, however, multi-axis goniometers were almost abandoned after the arrival of two-dimensional detectors, which restricted motions around the sample, due to the risk of collision. In addition, these goniometers never met the specifications imposed by the trend towards collecting on ever smaller crystals with ever smaller X-ray beam sizes. Their presence at third-generation synchrotrons was thus limited to few beamlines (Rosenbaum *et al.*, 2006; Shi *et al.*, 2006; Ascone *et al.*, 2007) until collision issues were addressed with the development of an inverse mini-kappa goniometer head with dedicated control software at ESRF/EMBL Grenoble (Brockhauser *et al.*, 2011). Several such systems have been



OPEN ACCESS

installed at synchrotron beamlines (Brockhauser *et al.*, 2013) but the vast majority of data sets remain collected from a single axis, primarily around ω .

Developed at the Swiss Light Source (SLS) at Paul Scherrer Institute, the Parallel Robotics Inspired Goniometer (PRIGo) (Gletting *et al.*, 2009, 2011) is a new type of multi-axis goniometer with high-end features such as micrometer precision around the main rotation axis ω , a large collision-free angular range, reduced self-shadowing and low-maintenance device mechanics. Fully integrated into the beamline software architecture, it enables the realisation of advanced data collection protocols for both native and experimental phasing experiments in a user-friendly manner. Herein we present the geometric model, calibration and accuracy of the PRIGo goniometer as well as its integration at beamline X06DA (PXIII)¹ at SLS. New opportunities for anomalous diffraction data collection are also presented.

2. Hardware and software description of PRIGo

Based on a combination of serial and parallel kinematics, PRIGo is a compact and precise multi-axis goniometer, which emulates the movements of an arc (Fig. 1). PRIGo utilizes linear and rotary piezo positioners (SLC-P-2490, SLC-P-24120 and SR-P-2013-S, SmarAct GmbH) driven by a combined stick slip and direct current principle, with built-in linear encoders operating in closed loop and enabling nanometer resolution and positional reproducibility <10 nm. Three of the four linear positioners are parallel to the ω rotation axis and connected by spherical joints to a tetrahedron-shaped platform, called the ‘Orion table’ (Henein, 2000) (Fig. 2). The fourth positioner is inclined by an angle of 18° and connects a swing head supporting the φ rotational stage. PRIGo is mounted on an air-bearing rotary stage (Aerotech ABRS-250) used for the ω rotation with a 36-channel slip-ring in the center enabling unlimited rotary motion. Translations at the sample position, as well as the χ rotation, are achieved with synchronous movements of the four linear positioners.

PRIGo’s control system was implemented in the Orchestra Control Engine², an open-source real-time control framework running on RTAI/Linux, which provides powerful and stable performance in a low-cost package. The various software modules of PRIGo (Fig. 3) communicate with a simple and efficient set of commands, keeping the network overhead to a minimum. PRIGo’s movements are described in the beamline coordinate system (see insert ‘measurement setup’ on Fig. 4), which does not correspond to linear movements of the individual motors. The conversion between the beamline coordinates ($x, y, z, \omega, \chi, \varphi$) and the motor positions (four linear positioners, ω and φ rotation stages) is achieved by a forward and inverse kinematics calculation. Performed by the control system at every cycle of the control loop (every 1 ms), this calculation ensures synchronized and smooth movements of the linear positioners.

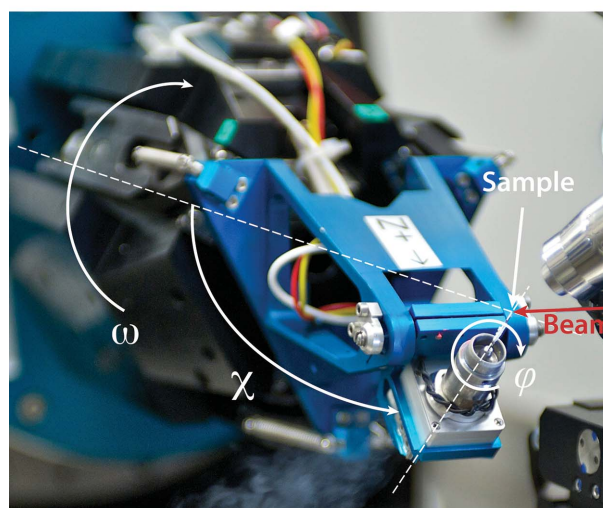
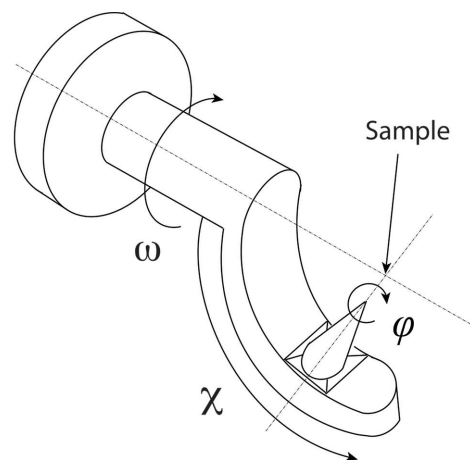


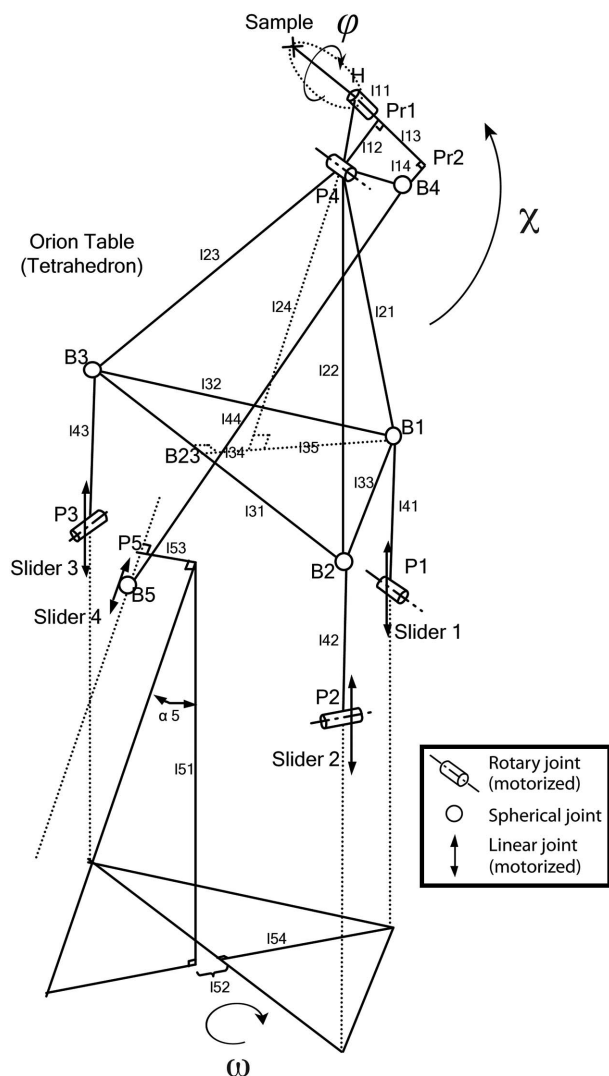
Figure 1
The PRIGo goniometer as mounted at beamline X06DA (PXIII) at SLS. The sketch of an arc (top) and a photograph of PRIGo at beamline X06DA (PXIII) at SLS (bottom) are represented with the ω , χ and φ angles overlaid. The beamline coordinate system is as follows: the X axis is along the spindle or ω axis, the Y axis is oriented vertically upward, and the Z axis is along the beam direction.

3. Calibration of PRIGo

The geometric model of PRIGo has 21 independent parameters, which correspond to PRIGo’s real dimensions (Fig. 2). Most could be measured using a three-dimensional coordinate-measuring machine (Wenzel LKS) with a precision of $\sim 10 \mu\text{m}$, yielding the relative position of the four linear positioners (positions B1 to B5 on Fig. 2). The parameters linked to the fourth linear positioner (slider 4 on Fig. 2), which have the largest effect on the geometric model, were then refined in an iterative manner by minimizing the sphere of confusion (SoC) for the χ rotation axis ($0\text{--}90^\circ$). Such SoC measurements were performed using a precise stainless steel reference sphere ($\varnothing = 12.7 \text{ mm}$) with form tolerance below $0.25 \mu\text{m}$, representing the sample mounted on the PRIGo sample holder and three capacitive sensors (Probe Type: C23/B, Driver System: Elite Series CPL190, Lion Precision/IBS Precision Engineering) aligned with the beamline coordinate system (Fuchs *et al.*, 2014) (Fig. 4). The same SoC measure-

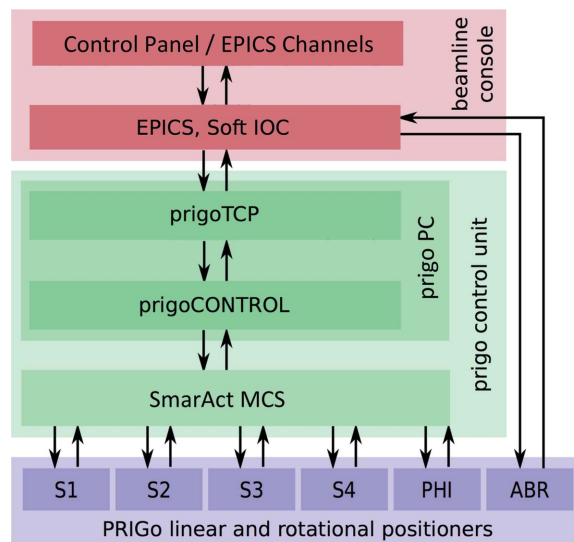
¹ X06DA (PXIII), <http://www.psi.ch/sls/pxiii/>.

² Orchestra, http://en.wikipedia.org/wiki/Orchestra_Control_Engine.


Figure 2

Kinematic structure of PRIGo. The PRIGo mechanism is driven by four linear positioners (or sliders), three of which are connected *via* a leg, comprising a pivot hinge and a ball joint, to a central tetrahedron shaped part, the so-called ‘Orion table’. The fourth linear positioner is responsible for tilting the φ rotation stage. Translations at the sample position, as well as the χ rotation, are achieved with synchronous movements of all four linear positioners. The φ stage rotates the sample around the sample holder axis, whereas the ω rotation can be performed by any conventional rotary stage. Numbered PRIGo parameters are preceded by I.

ments were also performed for the ω (0–360°) and φ (0–360°) rotation axes. We obtained a ‘geometric model’ peak-to-peak SoC of $5\ \mu\text{m}$, 25 $\mu\text{m}</math> and 10 $\mu\text{m}</math> for ω , χ and φ , respectively (Fig. 4, left side). To further improve these results, we implemented an active correction of the four motor positioners for the rotations around the ω (when $\chi = 0^\circ$) and χ axes (no correction was implemented for the φ axis yet). The active correction consists of parameterizing the measured deviation for a rotation (here, ω and χ), *i.e.* fitting a function to the SoC measurements. The deviations for the ω and χ rotations are described by a sum of two sinusoids (six parameters) and by a quadratic polynomial (five parameters), respectively. Implemented in the PRIGo control system, the active correction$$


Figure 3

PRIGo software. The schematic shows the different modules of PRIGo’s software and their interactions (represented by arrows). PRIGo’s control system receives commands from the input/output control servers (IOC) of the EPICS framework, which also controls the other beamline components including the air-bearing rotary stage (ABR). Within the PRIGo control unit, a transmission control protocol (TCP) server handles all communication (commands and feedback) over a TCP socket connection. The TCP server also receives the ABR ω position *via* EPICS, which is used by the PRIGo control to perform the active correction (see §3). The SmarAct positioners (S1–S4: SmarAct positioners, PHI: SmarAct rotary stage) feedback loop is controlled by the modular control system (MCS) from SmarAct GmbH.

around the ω axis is applied up to a speed of 180° s⁻¹. To achieve this, it is necessary to interpolate the position of the air-bearing rotary stage (ABR) ω position, which is obtained *via* EPICS (Fig. 3) at a rate of 10 Hz only. This is done within the calibration module of the PRIGo control, knowing the last ABR ω position and the rotation speed. The active correction is applied around the χ axis up to a speed of 5° s⁻¹.

Owing to the high resolution and repeatability of the SmarAct positioners as well as the reproducibility of PRIGo’s mechanics, the SoC improved to $1\ \mu\text{m}$ for ω and $7\ \mu\text{m}$ for χ (Fig. 4, right side). This accuracy is valid within $\pm 2.5\ \text{mm}$ deviation along x , y and z from the ideal sample position. The calibration, together with the active correction, have proven to be extremely stable over time and were repeated only once after 15 months of operation, following the maintenance of two linear positioners.

4. Integration of PRIGo at beamline X06DA (PXIII) at SLS

PRIGo was installed at beamline X06DA (PXIII) at the Swiss Light Source in January 2012 and is now fully integrated into the new data acquisition user interface DA+ (E. Panepucci *et al.*, unpublished). Its compact design and small space envelope at large χ angles (Maag *et al.*, 2013) (Fig. 5) maximize the achievable angular range but self-shadowing on the detector and potential collisions with beamline devices such as the collimator or the beam stop still impose angular restrictions.

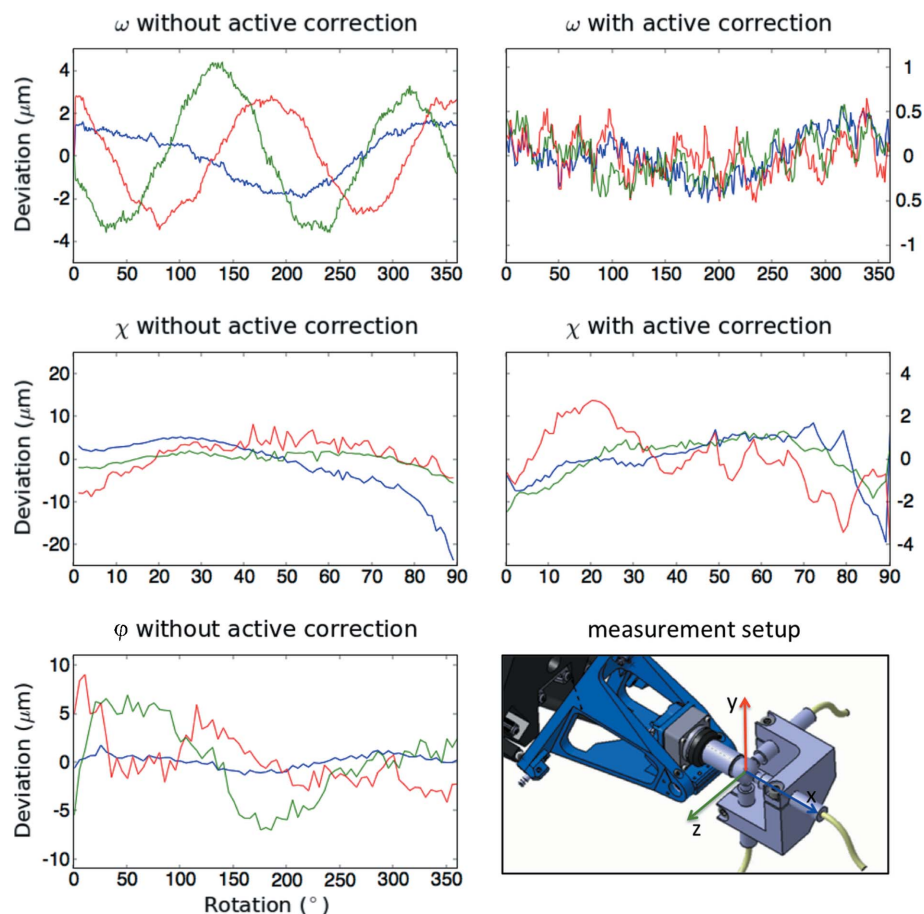


Figure 4 PRIGo's sphere of confusion measurements for ω , χ and φ rotation axes. PRIGo SoC measurements and calibration were performed with three capacitive sensors aligned with the beamline coordinate system (see 'measurement setup' insert) and a metal sphere representing the sample. The plots represent the SoC obtained by optimization of PRIGo's geometric model (without active correction) and after the implementation of an active correction (with active correction). The deviations along x , y and z from the ideal sample position are indicated in blue, red and green, respectively. During the measurement of an axis, the other two were kept at an angle of 0° . There is currently no active correction implemented for the φ axis. All SoC measurements were performed at 1° s^{-1} and reproducible within 200–300 nm.

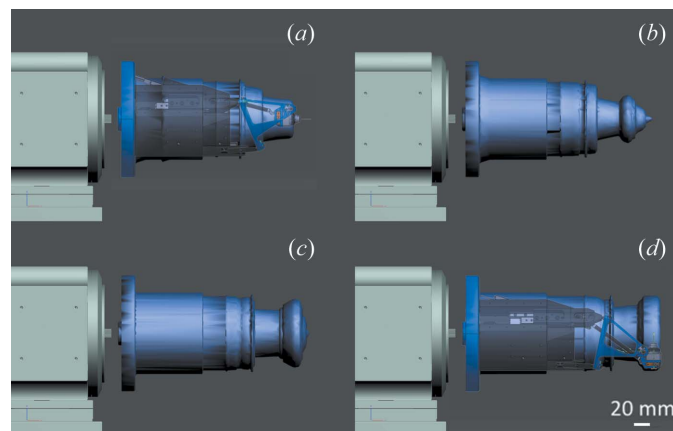


Figure 5 PRIGo space envelopes for full ω turns with different χ -offsets. Envelopes are shown for increasing χ values of (a) 0° , (b) 30° , (c) 60° and (d) 90° . A view of PRIGo with a sample at the tip (standard 18 mm pin) is overlaid for (a) and (d) for better visualization of the goniometer's parts.

Currently, PRIGo offers collision-free ω rotation with a χ angle up to 40° , more than 210° ω rotation with a χ angle between 40° and 60° , and more than 120° ω rotation with a χ angle of 90° (Fig. 6). The cryogenic nitrogen gas blowing directly on parts of PRIGo (mainly the head) can result in deflection of the device and movement at the sample position ($\sim 10 \mu\text{m}$). This is not of practical concern at beamline X06DA (PXIII) because the cryojet is oriented such that the affected positions are limited (light blue on Fig. 6), and in the cryo-stream for only a short time ($\sim 20 \text{ s}$) in a typical 360° data collection at a speed of 2° s^{-1} .

In addition, the PRIGo φ axis can also serve as a data collection axis (Table 1) thanks to continuous shutterless data acquisition capabilities offered by fast readout detectors such as the PILATUS (Broennimann *et al.*, 2006; Henrich *et al.*, 2009). Finally, PRIGo is compatible with both sample changer usage [an IRELEC CATS system with vial mounting is in place at X06DA (PXIII)] and manual transfer where a χ offset can facilitate both crystal mounting and recovery. Possible bump or collision on PRIGo upon sample exchange (from either robot or manual mounting) are recovered with an initialization procedure, which brings back all linear positioners to their reference positions. This procedure is completed in about 10 s.

5. Applications

Multi-axis goniometers like PRIGo are beneficial in a wide variety of cases including a simple reorientation to rotate around the crystal's best spot or data collection while avoiding contamination from satellite crystals. Other advantages are the unambiguous space group determination, alignment of a long crystallographic axis along the spindle in order to avoid overlapping reflections or minimization of the total oscillation range needed for a complete data set on a radiation-sensitive crystal (Brockhauser *et al.*, 2013). For crystals diffracting to atomic resolution, data measured at a different χ angle to collect the 'missing cusp' yield complete data in the highest-resolution shell after merging.

Multi-axis goniometers also enable optimal strategies for the measurements of anomalous diffraction data. In the case of single-wavelength anomalous dispersion (SAD) requiring high multiplicity (Dauter *et al.*, 1999), they provide an elegant way to acquire true redundant data (Debreczeni *et al.*, 2003)

Table 1

Data collection and processing statistics of a lysozyme crystal collected with PRIGo at beamline X06DA (PXIII).

Data sets of 360° were collected on a PILATUS 2M-F detector from a single lysozyme crystal in three different ways: around the ω axis ('traditional' rotation axis), around the φ axis with a χ angle of 0° (*i.e.* similar to the data collection around ω), and around the φ axis with a χ angle of 90° (simulating a vertical axis). The three data sets were collected in an interleaving manner with 90° wedges in order to distribute the X-ray dose evenly. Still, small effects of radiation damage can be observed in the processing statistics in the last resolution shell. An expected lower completeness was observed for the 'vertical axis' data as a result of both Lorentz and polarization corrections.

Data sets	Around ω	Around φ with $\chi = 0^\circ$	Around φ with $\chi = 90^\circ$ (‘vertical axis’)
Space group		$P4_32_12$	
Unit cell		$a = 78.3 \text{ \AA}, b = 78.3 \text{ \AA}, c = 37.2 \text{ \AA}$	
Beamline		X06DA (PXIII) / SLS	
Wavelength (Å)		1.0	
Overall / inner / outer resolution shells (Å)		39.1–1.2 / 39.1–10.0 / 1.3–1.2	
Completeness (%)	99.9 / 99.8 / 99.6	99.9 / 99.8 / 99.1	97.9 / 99.8 / 91.2
R_{meas} (%)	3.3 / 2.0 / 87.5	3.5 / 2.1 / 96.1	3.3 / 2.1 / 101.7
$I/\sigma(I)$	46.1 / 151.3 / 3.6	43.8 / 144.9 / 3.2	42.9 / 140.7 / 2.6
CC(1/2)	100.0 / 100.0 / 89.3	100.0 / 100.0 / 87.0	100.0 / 100.0 / 79.7
Reflections: measured	875773	877808	725366
unique	36675	36680	35958

with improved accuracy by changing the crystal orientation (here, multiple low-dose 360° data sets at various χ and φ angles). We successfully implemented such a strategy at beamline X06DA (PXIII) at SLS (Weinert *et al.*, 2015) and solved, using only the anomalous signal of low-Z elements and a single crystal entity, a 266 kDa multiprotein–ligand tubulin complex (Prota *et al.*, 2013) (T_2R -TTL) (Fig. 7). With 2317 residues, this is the largest structure solved by native-SAD phasing to date.

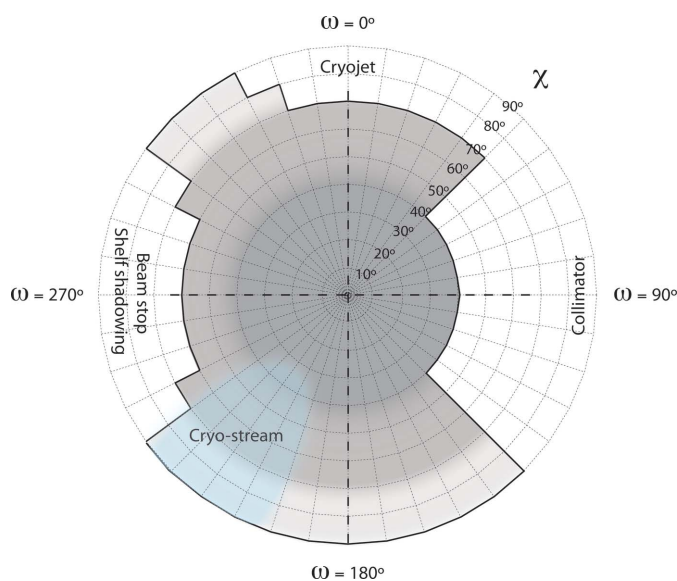


Figure 6
PRIGo collision and shadowing map at beamline X06DA (PXIII). Allowed χ angles with respect to the ω axis are shown in grey. 360° data can be collected around ω with a χ angle up to 40° (dark grey), more than 210° with a χ angle between 40° and 70° (medium grey), and more than 120° with a χ angle of 90° (light grey), respectively. Beamline devices with potential collision are indicated together with the position of the cryo-stream (light blue).

In the case of multiple-wavelength anomalous dispersion (MAD) experiments, PRIGo can be used to align an even-fold symmetry axis parallel to the spindle in order to collect *Bijvoet* mates on the same image, *i.e.* with essentially similar X-ray dose and absorption effects (Kahn *et al.*, 1985; Hendrickson *et al.*, 1988). For this, we use *XOalign* (Legrand, 2009) with an orientation matrix from indexed diffraction patterns to calculate possible goniometer angles compatible with the beamline collision map (Fig. 6). Phasing experiments can also be designed to take advantage of the anisotropy of the anomalous signal at an absorption edge (Bricogne *et al.*, 2005; Schiltz & Bricogne, 2008, 2010). Here, the possibility offered by PRIGo to collect data around the φ axis and to orient this axis at a chosen angle with respect to the

X-ray beam polarization is potentially a great advantage.

In conclusion, with a large angular range and micrometer precision, we have shown that the multi-axis goniometer PRIGo offers new possibilities for optimizing MX data collection protocols. By facilitating multi-axis data acquisitions, we aim at encouraging crystallographers to measure data with the highest accuracy, especially when attempting to obtain phases experimentally.

Acknowledgements

The authors would like to thank Markus Vitins and Stephan Maag for their help in manufacturing PRIGo, and Katja Bargsten, Natacha Oliéric, Andrea Prota and Michel Steinmetz for providing the T_2R -TTL crystals.

References

Ascone, I., Girard, E., Gourhant, P., Legrand, P., Roudenko, O., Roussier, L. & Thompson, A. W. (2007). *AIP Conf. Proc.* **872**, 874.

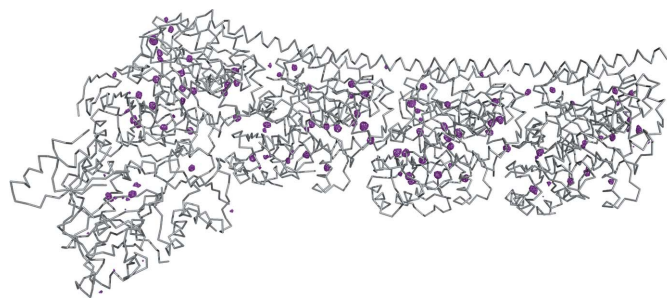


Figure 7
 α -trace of the T_2R -TTL complex (Prota *et al.*, 2013) and the anomalous difference Fourier map at 5σ . The anomalous difference map (magenta) shows the presence of 118 sulfur, 13 phosphorus, 3 calcium sites, 2 chloride sites in the multiprotein–ligand complex.

- Blake, C. C. F. & Phillips, D. C. (1962). *Vienna Int. At. Energ. Agency*. pp. 183–191.
- Bricogne, G., Capelli, S. C., Evans, G., Mitschler, A., Pattison, P., Roversi, P. & Schiltz, M. (2005). *J. Appl. Cryst.* **38**, 168–182.
- Brockhauser, S., Ravelli, R. B. G. & McCarthy, A. A. (2013). *Acta Cryst.* **D69**, 1241–1251.
- Brockhauser, S., White, K. I., McCarthy, A. A. & Ravelli, R. B. G. (2011). *Acta Cryst.* **A67**, 219–228.
- Broennimann, Ch., Eikenberry, E. F., Henrich, B., Horisberger, R., Huelsen, G., Pohl, E., Schmitt, B., Schulze-Briese, C., Suzuki, M., Tomizaki, T., Toyokawa, H. & Wagner, A. (2006). *J. Synchrotron Rad.* **13**, 120–130.
- Dauter, Z. (1999). *Acta Cryst.* **D55**, 1703–1717.
- Dauter, Z. (2005). *Prog. Biophys. Mol. Biol.* **89**, 153–172.
- Dauter, Z. (2010). *Acta Cryst.* **D66**, 389–392.
- Dauter, Z., Dauter, M., de La Fortelle, E., Bricogne, G. & Sheldrick, G. M. (1999). *J. Mol. Biol.* **289**, 83–92.
- Debreczeni, J. É., Bunkóczi, G., Ma, Q., Blaser, H. & Sheldrick, G. M. (2003). *Acta Cryst.* **D59**, 688–696.
- Fuchs, M. R., Pradervand, C., Thominet, V., Schneider, R., Panepucci, E., Grunder, M., Gabadinho, J., Dworkowski, F. S. N., Tomizaki, T., Schneider, J., Mayer, A., Curtin, A., Olieric, V., Frommherz, U., Kotrle, G., Welte, J., Wang, X., Maag, S., Schulze-Briese, C. & Wang, M. (2014). *J. Synchrotron Rad.* **21**, 340–351.
- Garman, E. F. & Weik, M. (2011). *J. Synchrotron Rad.* **18**, 313–317.
- Gletting, W., Henein, S., Breguet, J.-M. & Schulze-Briese, C. (2009). *Proceedings of the 9th Euspen International Conference*, pp. 192–195, San Sebastian, Spain.
- Gletting, W., Vitins, M., Schwarb, A., Maag, S. & Schulze-Briese, C. (2011). *Proceedings of the 11th Euspen International Conference*, pp. 31–34, Como, Italy.
- Helliwell, J. (1992). *Macromolecular Crystallography with Synchrotron Radiation*. Cambridge University Press.
- Hendrickson, W. A., Smith, J. L., Phizackerley, R. P. & Merritt, E. A. (1988). *Proteins*, **4**, 77–88.
- Henein, S. (2000). Thesis. EPFL, Switzerland.
- Henrich, B., Bergamaschi, A., Broennimann, C., Dinapoli, R., Eikenberry, E. F., Johnson, I., Kobas, M., Kraft, P., Mozzanica, A. & Schmitt, B. (2009). *Nucl. Instrum. Methods Phys. Res. A*, **607**, 247–249.
- Holton, J. M. & Frankel, K. A. (2010). *Acta Cryst.* **D66**, 393–408.
- Kahn, R., Fourme, R., Bosshard, R., Chiadmi, M., Risler, J. L., Dideberg, O. & Wery, J. P. (1985). *FEBS Lett.* **179**, 133–137.
- Legrand, P. (2009). *xdsmc*, <http://code.google.com/p/xdsmc/>.
- Maag, S., Frommherz, U., Kotrle, G., Thominet, V., Welte, J., Pradervand, C., Thermer, R., Schnorf, D., Ellenberger, U. & Fuchs, M. R. (2013). *J. Phys. Conf. Ser.* **425**, 012009.
- Prota, A. E., Bargsten, K., Zurwerra, D., Field, J. J., Díaz, J. F., Altmann, K.-H. & Steinmetz, M. O. (2013). *Science*, **339**, 587–590.
- Ravelli, R. B. G. & Garman, E. F. (2006). *Curr. Opin. Struct. Biol.* **16**, 624–629.
- Rosenbaum, G., Alkire, R. W., Evans, G., Rotella, F. J., Lazarski, K., Zhang, R.-G., Ginell, S. L., Duke, N., Naday, I., Lazarz, J., Molitsky, M. J., Keefe, L., Gonczy, J., Rock, L., Sanishvili, R., Walsh, M. A., Westbrook, E. & Joachimiak, A. (2006). *J. Synchrotron Rad.* **13**, 30–45.
- Schiltz, M. & Bricogne, G. (2008). *Acta Cryst.* **D64**, 711–729.
- Schiltz, M. & Bricogne, G. (2010). *Acta Cryst.* **D66**, 447–457.
- Shi, W., Robinson, H., Sullivan, M., Abel, D., Toomey, J., Berman, L. E., Lynch, D., Rosenbaum, G., Rakowsky, G., Rock, L., Nolan, B., Shea-McCarthy, G., Schneider, D., Johnson, E., Sweet, R. M. & Chance, M. R. (2006). *J. Synchrotron Rad.* **13**, 365–372.
- Weinert, T. *et al.* (2015). *Nat. Methods*, **12**, 131–133.